PCCP

Accepted Manuscript

ROYAL SOCIETY OF CHEMISTRY

www.rsc.org/pccp

PCCP

RSCPublishing

ARTICLE

Destabilization effect of transition metal fluorides on sodium borohydride

Cite this: DOI: 10.1039/xoxxoooooox

Georgios N. Kalantzopoulos[a], Matylda N. Guzik[a], Stefano Deledda[a], Richard H. Heyn[a], Jiri Muller[a] and Bjørn C. Hauback[a,*]

Received ooth January 2012,
Accepted ooth January 2012

DOI: 10.1039/xoxxoooooox

www.rsc.org/

The effect of transition metal fluorides on the decomposition of $NaBH_4$ has been investigated for $NaBH_4$ ball milled with TiF_3, MnF_3 or FeF_3. The compounds were examined by thermal programmed desorption with residual gas analysis, thermo gravimetric analysis and volumetric measurements using a Sieverts-type apparatus. The phase formation process during thermal decomposition was studied by *in situ* synchrotron radiation powder X-ray diffraction on the as-milled powders. $NaBF_4$ was among the products in all mechano-chemical reactions. ^{11}B-NMR spectra analysis gave $NaBF_4$:$NaBH_4$ ratios of 1:150 for Na-Ti, 1:40 for Na–Mn, and 1:10 for Na–Fe. Pure $NaBH_4$ possessed a hydrogen release onset temperature of 430 °C. The hydrogen release in the $NaBH_4$ - MnF_3 system began as low as 130 °C. FeF_3 decreased the onset temperature to 161 °C and TiF_3 to 200 °C. TiF_3 reacted completely with $NaBH_4$ below 320 °C. All the examined systems have negligible emissions of diborane species. H-sorption studies performed at selected temperatures above 300 °C exhibited relatively fast desorption kinetics. Partial hydrogen re-absorption was observed for the Na–Mn and Na–Fe samples.

[a]*Institute for Energy Technology, P.O. Box 40, N-2027, Kjeller, Norway.*
[b]*SINTEF Materials and Chemistry, P.O. Box 124 Blindern, N-0314 Oslo, Norway.*

1 Introduction

Hydrogen is the most abundant element in the universe and it can be used in a variety of applications as an energy carrier. The molecular form of hydrogen contains three times more energy per mass than hydrocarbons [1, 2] making it an ideal alternative to fossil fuels for energy storage. In addition, when hydrogen reacts with oxygen to produce energy (e.g. in a fuel cell), H_2O is the only by-product [3].

Borohydrides, boron-containing complex hydrides which can be synthesized either by wet-chemistry methods or by solid-state synthesis[4], have attracted a lot of attention within the hydrogen storage community due to their high content of H_2 [5, 6]. Research has addressed both synthesis of novel compounds and understanding of the decomposition path of borohydrides [7-9]. Release of B-H (borane) species can be observed during the decomposition of some transition metal borohydrides $M_{n-1}(BH_4)_n$ (M=Zn, Mn, Al, n=2, 3, 4) and in particular those with decomposition temperature below 200 °C [8]. This is a drawback for the reversibility of the systems [10]. Another drawback is the relatively high thermodynamic stability of most borohydrides. For this reason, different strategies for destabilizing borohydrides have been explored: anion substitution, cation substitution, mixed metal borohydrides, nanoconfinement, and synthesis of reactive hydride composites [5, 11-13]. Anion substitution was first reported as a destabilizing method on Na_3AlH_6 [14] and has been proposed as a promising method to tailor the thermodynamics of complex hydrides [15-25]. Recently, we reported the first F-substitution observed in borohydrides, by ball-milling KBH_4 with KBF_4 [26]. In the $NaBH_4$-$NaBF_4$ system the substitution takes place at between 200 – 215 °C [25] and the latter two works were published almost at the same time. Cation substitution has been reported for $Mg_{(1-x)}Zn_x(BH_4)_2$ (x=0.3-0.4), $Mg_xMn_{(1-x)}(BH_4)_2$ (x=0-0.8) and $LiMn(BH_4)_3$/2LiCl. For those systems, a clear decrease of the decomposition temperature has been observed [5, 12, 27-30]. For $LiCe(BH_4)_3Cl$, the simultaneous substitution of both the anionic and cationic part has been achieved creating a compound with a significantly reduced decomposition temperature and improved kinetics [31, 32]. Very recently it has been shown that rare-earth (RE) borohydrides with RE = La to Gd have both anionic and cationic substitution while RE = Yb and Lu form double-cation compounds [33, 34].

Among the various borohydrides, $NaBH_4$ is a promising hydrogen storage material due to its high gravimetric hydrogen capacity (10.4 wt%). However, its use for mobile or stationary applications is challenging due to its high thermodynamic stability and lack of reversibility. The room temperature (RT) α-phase of $NaBH_4$ has cubic symmetry (space group *Fm*-3*m*) [35].

Two competing decomposition overall reactions have been proposed [36].

$$NaBH_4 \longrightarrow Na + B + 2H_2 \quad (1)$$

and

$$NaBH_4 \longrightarrow NaH + B + 3/2H_2 \quad (2)$$

Hydrogen release starts at approximately 150 °C and becomes more significant above 470 °C. Urgnani *et al.* proposed a multistep mechanism involving the decomposition of $NaBH_4$ between 150 and 400 °C, although they observed only X-ray diffraction peaks related with unreacted $NaBH_4$ in this temperature region [36]. Above 475 °C $NaBH_4$ is shown to be in a liquid state [37]. The complete decomposition of $NaBH_4$ takes place at 505 °C, and the process does not involve evolution of B_2H_6 or other borane (B-H) species[24].

There are limited studies on the effect of Transition Metal Fluorides (TMFs) on the thermodynamic and kinetic properties of hydrides. Most of the work has focused on their catalytic effect on MgH_2 [38, 39]. It has been demonstrated that H absorption/desorption kinetics are enhanced due to the presence of the fluoride anion [40, 41], and that the fluorides have stronger catalytic effect on MgH_2 than the analogous chlorides [42]. To our knowledge, there are only a few studies on the effect of TMFs on the structure, sorption kinetics and thermodynamics of borohydrides. Recently it was found that the mechano-chemical reaction between $NaBH_4$ and ZnF_2 creates a mixture with favorable H-sorption kinetics below 100 °C [43]. No cation exchange reaction was observed. However for $ZnCl_2$ mixed with $Zn(BH_4)_2$ chloride substitution takes place [44]. Chloride substitution was also observed after ball milling of $NaBH_4$ with other transition metal chlorides and was found to be independent of the milling conditions [20, 24]. Very recently, we observed partial reversibility with slow kinetics for $NaBH_4$ with different Ni-containing additives [45].

So far little understanding on the mechanism of the fluoride additives has been achieved. It has been shown that TiF_3 doping decreases the decomposition temperature of the $NaBH_4/MgH_2$ system by 100 °C and improves the kinetics of hydrogen desorption [46]. Theoretical studies have indicated that the addition of Ti to $NaBH_4$ leads to the destabilization of the $[BH_4]^-$ anion [47].

In the present study, the formation of mixed Na-transition metal (TM) borohydrides with TM = Ti, Mn, Fe is evaluated. Furthermore, the effect of TMFs on the structure and decomposition behavior of $NaBH_4$ has been examined including an investigation of the formation of intermediate products and understanding of their role in the pure material decomposition. Results from thermogravimetric analysis are compared with *in situ* synchrotron radiation powder X-ray diffraction data in order to shed light on the effect of selected fluorides on the decomposition steps of $NaBH_4$. The dehydrogenation profile of the decomposition process is presented and discussed with respect to the intermediate phases observed during decomposition.

2 Experimental

Materials

Commercial $NaBH_4$ powder (99 % purity) as well as transition metal fluorides, TiF_3 (99 % purity), MnF_3 (99.9 % purity) and FeF_3 (98 % purity), were purchased from Sigma-Aldrich.

Sample preparation

Mixtures of $NaBH_4$ and TMF_3, TM= Ti, Fe with a molar ratio 4:1 and Mn with a molar ratio 4.8:1, were ball-milled in a Fritsch Pulverisette 6 Monomill at 400 rpm, for 3 h, under 1 bar of Ar gas using stainless steel balls and vials (ball-to-powder ratio 100:1). A mixed alkali-transition metal borohydride has been formed for molar ratios above 3:1 for example in $LiCe(BH_4)Cl$ and $NaZn(BH_4)_3$ [31, 48]. All sample handling and preparation were carried out under inert atmosphere of Ar in an MBraun Unilab glove box fitted with a recirculation system and gas/humidity sensors. Oxygen and water levels were kept below 1 ppm at all times.

Initial sample characterization

All samples were initially investigated by powder X-ray diffraction (PXD) using a Bruker D8 Advance diffractometer (Cu-K1, radiation) equipped with a Sol-X detector. Pure $NaBH_4$ was measured with a one-dimensional PSD (Lynxeye) detector. The powder samples were packed in 0.5 mm diameter boron-silica glass capillaries sealed with water-free glue under Ar.

Synchrotron Radiation Powder X-Ray Diffraction (SR-PXD)

In situ SR-PXD measurements were performed at the Swiss–Norwegian beamline (station BM01A) at the European Synchrotron Radiation Facility (ESRF) in Grenoble, France. The samples were kept under dynamic vacuum in a 0.5 mm boron-silica glass capillary. A gas blower was used to heat the samples from RT to 600 °C with a constant heating rate of 2 °Cmin^{-1}. Temperature calibration was performed by measuring a sample of pure Sn. The SR-PXD patterns (exposure time of 30 s) were collected using an image plate detector (MAR345) and then integrated by the Fit2D program[49]. The wavelengths, λ = 0.9339 Å for $NaBH_4$ + FeF_3 and $NaBH_4$ + TiF_3 and λ = 0.69674 Å for $NaBH_4$ + MnF_3, were calibrated from individual runs with LaB_6. For selected patterns, Rietveld refinements were performed with the Fullprof software [50]. The peak shapes were described by the pseudo-Voigt function and the background was modeled by using Fourier filtering procedure.

Thermogravimetric Analysis (TGA)

Experiments were performed with a Netzsch STA 449 F3 Jupiter instrument. The samples were measured in Al crucibles with pierced lids of the same material and heated between 30 and 600 °C, with a heating rate of 2 °C/min under argon gas (50 ml/min). The measurements were baseline corrected using the Proteus software package.

Sieverts' apparatus

Dehydrogenation and hydrogenation profile measurements were carried out in a calibrated in-house-built volumetric apparatus. Approximately 200 mg of material was inserted in a stainless steel sample holder and placed under static vacuum (10^{-5} mbar). During hydrogenation or dehydrogenation, the samples were heated from RT to the desired temperature at 20 °C/min and then held under isothermal conditions for at least 24 h. For hydrogenation, which was carried out at pressures between 135 and 142 bar, the samples were exposed to H_2 pressure at RT prior to heating. For the Na–Mn a fresh powder

sample was used for each desorption – absorption cycle at 260 and 360 °C, respectively.

Temperature-Programmed Desorption (TPD) with Residual Gas Analysis (RGA)

TPD data were collected with an in-house developed apparatus under vacuum (10^{-5} mbar) and between RT and 600 °C at a constant heating rate of 2 °C/min. Simultaneous RGA was measured with a MULTIVISON IP detector system coupled to a PROCESS Eye analysis package from MKS Instruments.

Nuclear Magnetic Resonance (NMR)

^{11}B NMR data were collected on a Bruker Advance III 500 MHz spectrometer operating at a frequency of 160.455 MHz. The spectra were obtained using a 4.0 mm MAS probe spinning at a rate of 10 kHz and 1.0 µs pulses at a 125 kHz rf-field with a recycle delay of 20 s. The chemical shifts of ^{11}B were externally referenced to $NaBH_4$ at -41.5 ppm.

3 Results

Synthesis and structural characterization

The ball-milling of $NaBH_4$ with TiF_3 did not result in the formation of new, crystalline phases (Figure 1a). The main phases found by PXD in the as-milled powder are $NaBH_4$ and TiF_3 which account for 87 and 12 wt.%, respectively, instead of the nominal 59 and 41 wt. % mixture composition (4:1 molar ratio) prior to milling. Additionally, minor amounts of TiB_2 and metallic Fe impurities are observed (below 1 wt.%). Neither the PXD patterns nor the ^{11}B NMR spectra (Figure 2) show any crystalline or amorphous titanium-boride phase as observed by XPS in a recent study of $NaBH_4$ and TiF_3 [51].

For the $NaBH_4$ with MnF_3, the most abundant phase in the as-milled powder is unreacted $NaBH_4$ (66 wt.%). The main new products after ball-milling are $NaBF_4$ (5 wt.%) and two different crystallographic polymorphs of MnF_2, tetragonal symmetry with space groups $P4_2/mnm$ and $P\text{-}42m$, and 1 and 28 wt.%, respectively (Figure 1b). Partial substitution of H^- with F^- in the $[BH_4]^-$ anion has recently been reported in the KBH_4 – KBF_4 system, resulting in a reduced enthalpy of decomposition [26]. In that work, the cubic symmetry of KBH_4 is retained and the substitution resulted in a larger unit cell volume. The present work does not show any substitution of F^- by H^-, and thus is in agreement with recent work showing that the substitution only takes place at elevated temperatures (200 – 215 °C) [25] and the substitution-derived compounds are not stable at RT for the $NaBH_4/NaBF_4$ mixture [25]. Most likely the observed MnF_2 were obtained by reduction of MnF_3.

The SR-PXD pattern of the as-milled $NaBH_4$ and FeF_3 at RT (Figure 1c) has a rather high background for $2\theta = 8 – 16°$, and thus indicating the presence of an amorphous fraction (see below). The RT data shows the formation of NaF (44 wt.%) and the presence of unreacted $NaBH_4$ (55 wt.%). Additionally, traces of the two polymorphs of metallic Fe (cubic symmetry, space group $Fm\text{-}3m$ and $Im\text{-}3m$) and FeF_3 are detected. Besides FeF_3, a possible origin of Fe can be the milling media. The fraction of FeF_3 has significantly decreased after milling, suggesting that the fluorine led to the formation of NaF. Since the majority of the starting Fe does not seem to be present in a crystalline form, it is very likely that it is partially bonded with B and exists in an amorphous state.

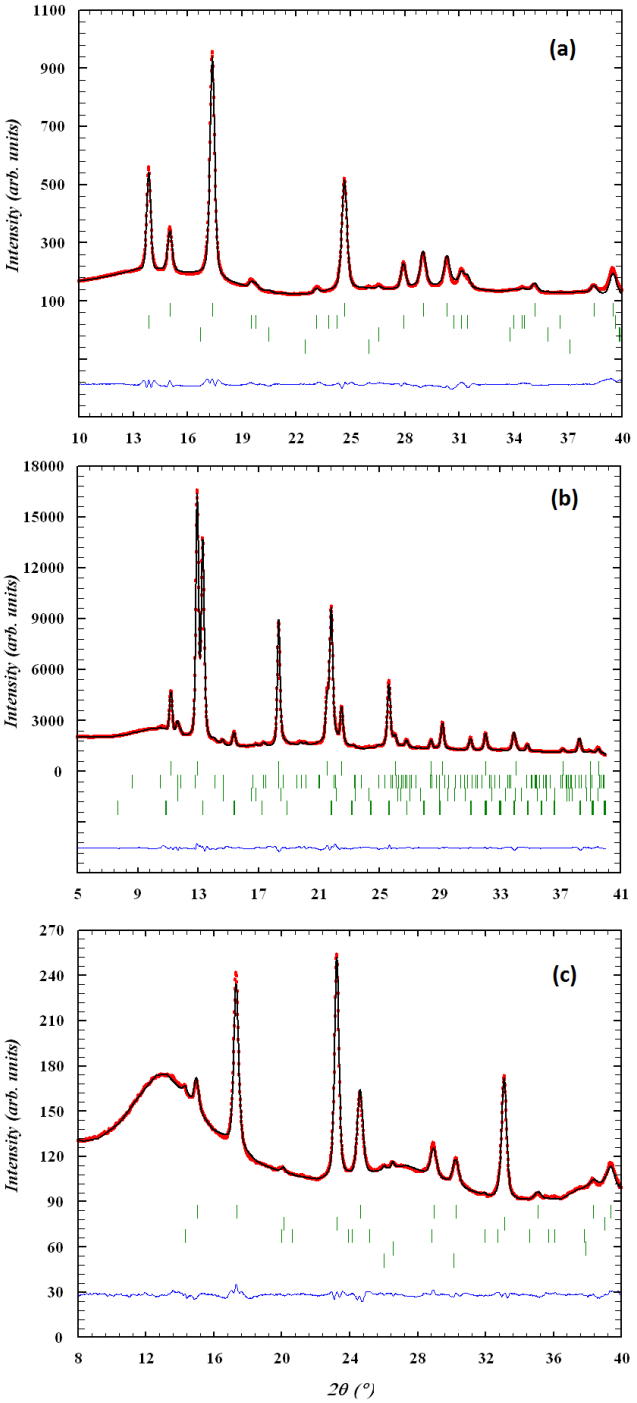

Figure 1: Rietveld refinement of SR-PXD data at RT for the as-milled: (a) $4NaBH_4 + TiF_3$, (b) $4.8NaBH_4 + MnF_3$, (c) $4NaBH_4 + FeF_3$. Dots represent the experimental data and the continuous line the Rietveld refinement. From top to bottom, green tick marks show (a): $NaBH_4$, TiF_3, TiB_2, Fe (b): $NaBH_4$, $NaBF_4$, MnF_2 ($P42/mnm$), MnF_2 ($P\text{-}42m$) and (c): $NaBH_4$, NaF, FeF_3, Fe ($Im\text{-}3m$), Fe ($Fm\text{-}3m$). The wavelengths are $\lambda = 0.9339$ Å for $4NaBH_4 + FeF_3$ and $4NaBH_4 + TiF_3$ and $\lambda = 0.69674$ Å for $4.8NaBH_4 + MnF_3$.

The ^{11}B-NMR spectra of the as-milled $NaBH_4$ with TiF_3, MnF_3, and FeF_3, respectively, show only $NaBH_4$ and $NaBF_4$ as the detectable products (Figure 2). Integration of these peaks gave $NaBF_4$:$NaBH_4$ ratios of 1:150 for Na-Ti, 1:40 for Na–Mn, and 1:10 for Na–Fe. These results suggest that the highest fraction of $NaBF_4$ is found in the Na-Fe sample, even if this sample does not show any diffraction peaks for $NaBF_4$ (Figure 1c). We can therefore assume that in this case $NaBF_4$ is present as an amorphous phase which contributes to the high background observed in the SR-PXD patterns. The relative lack of spinning side bands for the Na–Ti sample is suggestive of a more symmetric local environment for the $[BH_4]^-$ tetrahedra in this sample, in comparison to the Na–Mn and Na-Fe samples. The spectra show no indications of a M_xB_y (M = Ti, Mn, Fe) phase, but any paramagnetic M_xB_y phases would likely not be observable in the spectra and thus the presence of metal borides cannot be ruled out.

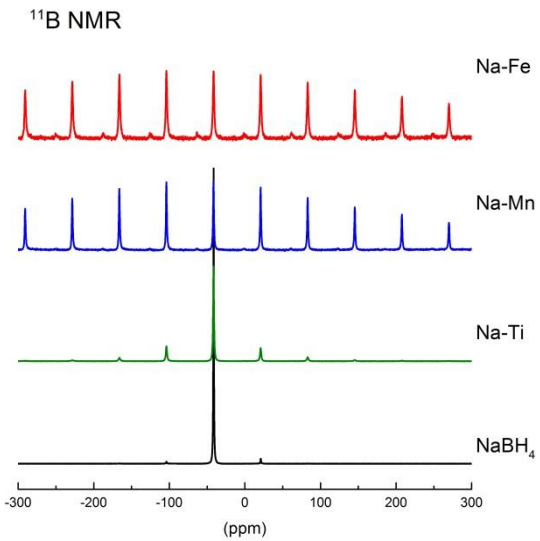

Figure 2: ^{11}B-NMR spectra for (a) pure $NaBH_4$ and the as-milled: (b) $4NaBH_4 + TiF_3$, (c) $4.8NaBH_4 + MnF_3$, (d) $4NaBH_4 + FeF_3$.

Thermal Decomposition

The *in situ* SR-PXD patterns of the Na-Ti system (Figure 3) remain unaltered from RT up to 220 °C. Above 220 °C the intensity of the peaks for TiF_3 and $NaBH_4$ decreases and a monoclinic phase identified as Na_3TiF_6 (space group $P2_1/c$) can be observed. Bragg peaks for NaF appear at 240 °C. At 260 °C TiF_3 is no longer detected, indicating its complete reaction with $NaBH_4$ to form Na_3TiF_6. Above 320 °C the Bragg peaks of Na_3TiF_6 are no longer observed. The $NaBH_4$ is only partially consumed during the reaction to form Na_3TiF_6. A substantial fraction is still observed above 260 °C and it decomposes as the temperature increases. The decomposition of the unreacted $NaBH_4$ is accompanied by the appearance of $NaBO_2$ at 320 °C (trigonal, space group R-3c), with new diffraction peaks observed at 2θ = 17.1, 19.4, 20.4, 24.1, 25.9 and 27.1°, respectively (Figure 3). The formation of borate phases during heating has been previously observed for $Ca(BH_4)_2$ [52]. Further increase in the temperature causes amorphization of $NaBO_2$ at ~360 °C. However, at about 510 °C it re-crystallizes with the same symmetry as above, and the remaining $NaBH_4$ is completely consumed. At 600 °C the sample consists of NaF (90 wt.%) and $NaBO_2$ (10 wt%). When cooling down to 300 °C the sample composition remains unchanged and the unit cell shrinking due to thermal contraction is the only phenomenon observed. In summary, Na_3TiF_6 forms from the reaction of $NaBH_4$ with TiF_3. The decomposition of Na_3TiF_6 appears to be strongly related with the formation of NaF.

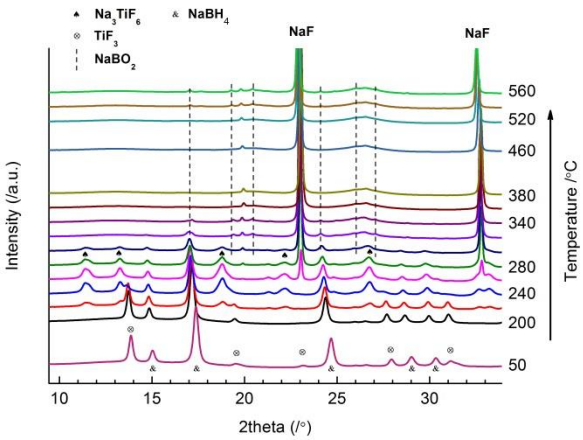

Figure 3: *In situ* SR-PXD of the Na – Ti system between 50 and 560 °C. Heating rate is 2 °C/min and λ = 0.9339 Å.

The *in situ* SR-PXD diffraction patterns of the as-milled Na-Mn system (Figure 4) show no changes up to 130 °C. At this temperature the Bragg peaks of $NaBF_4$ become less intense and they are completely absent at 230 °C. At 180 °C the formation of orthorhombic $NaMnF_3$ (space group *Pnma*) takes place, whereas the Bragg peaks of $NaBH_4$ lose intensity. Between 180 and 250 °C the more abundant fraction of MnF_2 (P-42m) decomposes completely, whereas the less abundant MnF_2 phase ($P2_1/mnm$) can no longer be observed above 200 °C. Above 230 °C the intensity of the NaF peaks increases. At 180 °C a new peak appears at 2θ = 12.4°. This can be assigned to Mn_2F_5 and is present in all diffraction patterns up to 450 °C. $NaMnF_3$ can be observed up to 400 °C, when it decomposes. Finally, also in this case, the formation of $NaBO_2$ associated with the decomposition of $NaBH_4$ can be observed at 420 °C. At 510 °C only three phases are present: $NaBO_2$ (46 wt.%), NaF (53 wt.%) and Mn_3O_4 (1 wt.%). The formation of the latter is observed from 420 °C. Similar to Na-Ti, these results suggest that $NaMnF_3$ forms from reaction of $NaBH_4$ with MnF_2. However, also $NaBF_4$ appears to participate in the formation of this ternary fluoride. As the temperature increases NaF formation appears to be related with $NaMnF_3$ decomposition.

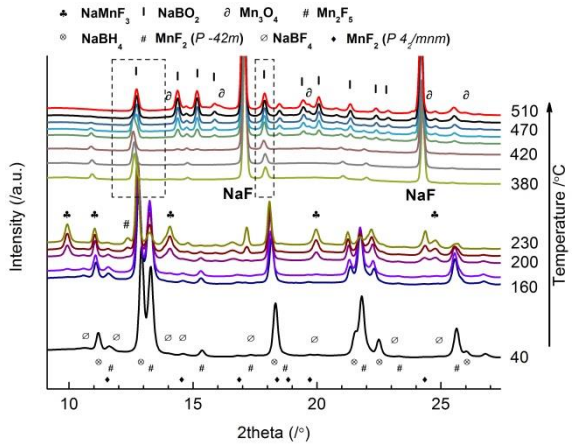

Figure 4: *In situ* SR-PXD of the Na – Mn system between 160 and 510 °C showing the formation of the intermediate phase $NaMnF_3$ and the formation of $NaBO_2$. Heating rate is 2 °C/min and λ = 0.69674 Å.

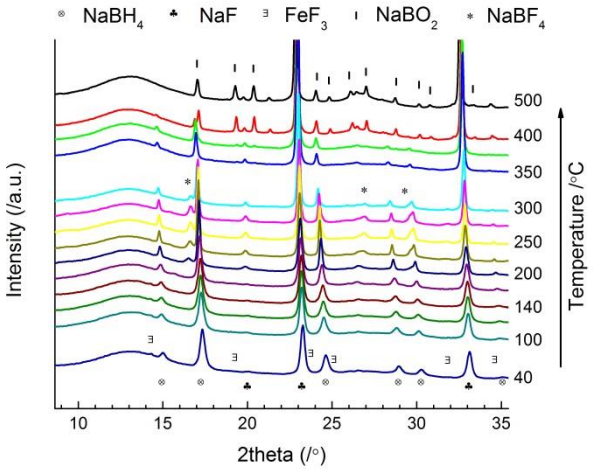

Figure 5: *In situ* SR-PXD of the Na – Fe system between 50 and 500 °C. Heating rate is 2 °C/min and λ = 0.9339 Å.

The relatively high background for 2θ = 8 – 16° shown in Figure 1c for the Na-Fe system is present in all patterns up to 500 °C (Figure 5) and suggests the existence of one or more amorphous phases. FeF_3 is not observed in diffraction patterns above 140 °C. At 200 °C the formation of an additional phase takes place. The new Bragg peaks can be most likely ascribed to the hexagonal modification of $NaBF_4$, however the space group and atomic coordinates are unknown [53]. It is worth noticing that $NaBF_4$ was observed by ^{11}B-NMR in the as-milled powder. Hence, we can ascribe these peaks to an amorphous-to-crystalline phase transition, rather than to the fresh formation of $NaBF_4$ polymorph during heating. The diffraction peaks for NaF, which are present in the sample from the very beginning, gain intensity above 250 °C whereas the $NaBH_4$ peaks remain unchanged up to 270 °C. Above this temperature their intensity starts decreasing, and at 415 °C they are no longer observed. $NaBF_4$ cannot be detected above 320 °C. At 370 °C the $NaBH_4$ peaks overlap with those of $NaBO_2$, as observed for Na–Ti and Na–Mn. Among the two Fe polymorphs seen in the RT pattern, only the bcc-Fe is observed until the very end of the heating process. At 500 °C three phases are identified: NaF (69 wt.%), $NaBO_2$ (30 wt.%) and bcc Fe (1 wt.%). During cooling from 500 to 300 °C the sample composition remains unchanged. $NaBO_2$ was formed in all the three samples in substantial percentage. The presence of O can be originated from impurities in the starting material, most likely the $NaBH_4$.

Thermogravimetric Analysis (TGA) and Thermal Programmed Desorption (TPD) with Residual Gas Analysis (RGA)

For all systems, TGA and TPD with RGA (Figure 6 and Figure 7, respectively) show a multistep decomposition mechanism, compared with the single-step decomposition observed for pure $NaBH_4$ (also included in the figures for comparison). The main species detected by RGA during the decomposition process is hydrogen (mass 2), whereas the signals of B-H species (masses 26 and 27) were two orders of magnitude weaker than the signal of mass 2 over the whole temperature range.

In the RGA spectrum of the Na-Ti system (Figure 7b), a first hydrogen release step occurs between 220 and 320 °C (region I in figure 7b). A second stage involves three overlapping peaks between 320 and 420 °C (region II in figure 7b). Compared to Na-Mn and Na-Fe (discussed below) this system has the narrowest gas release temperature range. From the TGA profile the partial reaction of $NaBH_4$ with TiF_3 to form Na_3TiF_6, which was observed during *in situ* SR-PXD, is accompanied by hydrogen desorption and a mass loss of 1.5 wt.%. Above 260 °C and up to 340 °C the mass loss is 2.3 wt.%. In this temperature region, Na_3TiF_6 decomposes to form NaF (SR-PXD data) and hydrogen is the only gas being emitted (TPD data). This suggests that the decomposition of Na_3TiF_6 could promote the decomposition of the remaining $NaBH_4$.

The RGA spectrum for Na-Mn consists of three main gas evolution regions (Figure 7c). A broad peak of very low intensity with onset at 135 °C is observed below 160 °C (region I in figure 7c). The onset of hydrogen release is the lowest among the present samples. This indicates a strong destabilization effect of MnF_2 on $NaBH_4$. The decomposition behavior observed by TGA is in agreement with the RGA spectrum. The broad, low-intensity peak observed in region I of the RGA spectrum (Figure 7c) can be associated to a 0.2 wt.% mass loss in the TGA, whereas the first gas evolution event consisting of two overlapping peaks between 160 and 230 °C (Region II in figure 7c) accounts for a mass loss of 2.0 wt.%. The latter can be associated with the reaction of $NaBH_4$ with MnF_2 to form the ternary fluoride $NaMnF_3$, as observed in the *in situ* SR-PXD data. The second main gas evolution step, between 230 and 280 °C (region III in figure 7c), accounts for a mass loss of 1.5 wt.%. At those temperatures, *in situ* SR-PXD shows the formation of NaF at the expense of $NaMnF_3$. No significant mass loss is observed until 390 °C (region IV in figure 7c) where the last gas evolution step accounting for 1.8 wt.% occurs.

Two main gas evolution regions are observed for the Na-Fe sample (Figure 7d). The first one has a double peak extending between 250 and 350 °C (region II); the second one also consists of two overlapping peaks and lies between 350 and 490 °C (region III). In this system, the onset temperature of the first hydrogen release is 161 °C (region I). This is 270 °C lower than in pure $NaBH_4$.

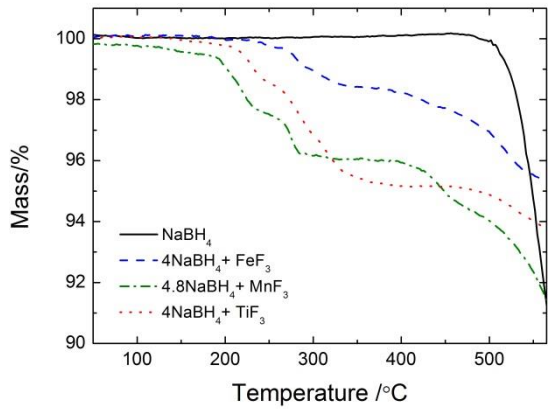

Figure 6: TGA of the as-milled systems. Heating rate is 2°C/min.

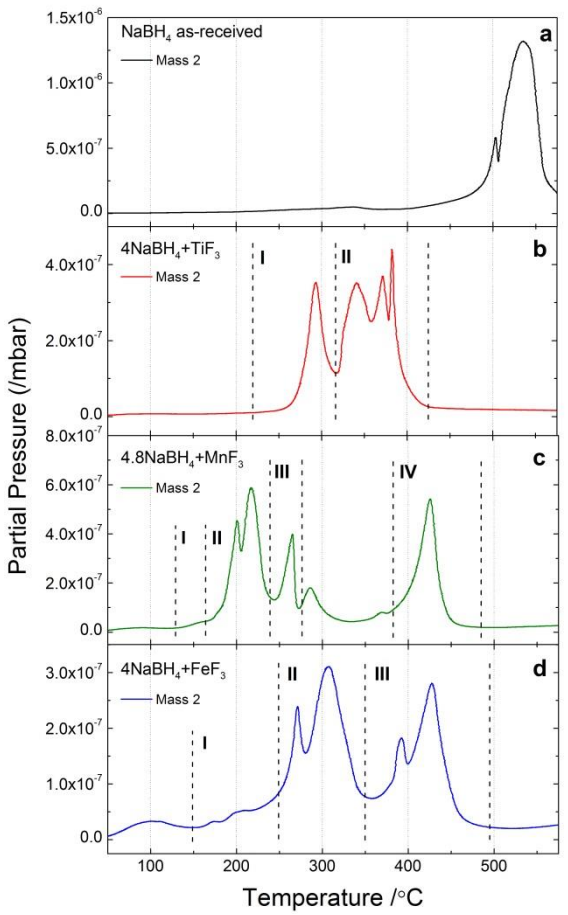

Figure 7: TPD with RGA from RT up to 575 °C of the as-milled samples. (a) pure $NaBH_4$, (b) $4NaBH_4$ + TiF_3, (c) $4.8NaBH_4$ + MnF_3, (d) $4NaBH_4$ + FeF_3. Heating rate is 2 °C/min. Only the signal for mass 2 (H_2) is shown.

Region I can be associated with a 0.5 wt.% mass loss on the TGA profile. TGA data shows a mass loss of 1.7 wt.% up to 350 °C (region I and II), whereas region III accounts for 1.5 wt.% mass loss. The latter can be associated with the decomposition of unreacted $NaBH_4$ as observed by *in situ* SR-PXD.

Decomposition Kinetics

The desorption and absorption behavior of the three systems were investigated at 345 °C for the Na-Ti system, 260 and 360 °C for Na-Mn and 445 °C for Na-Fe, respectfully. The selected temperatures correspond to the most significant desorption events observed by TPD for each sample. Hydrogen absorption experiments were carried out after each desorption. In order to clarify how the phase mixtures influence the kinetics and reversibility the presence of any $NaBH_4$ or other H-containing phase(s) were investigated in detail by PXD after absorption.
The decomposition profile of the Na-Ti sample is shown in Figure 8. The maximum H_2 amount desorbed for Na-Ti is 3.6 wt.% and it is reached 1.5 h after the heating begins. Further isothermal treatment in vacuum up to 20 h does not result in any additional gas desorption. Interestingly, 95% of the hydrogen release is achieved after 0.75 h. A closer look at the first 2 h (see inset Figure 8) reveals a first desorption event, occurring during heating before 275 °C, and a second event between 275 and 345 °C. These two steps are in good agreement with the TGA measurements (Figure 6). They are attributed to the reaction of partial amount of $NaBH_4$ with TiF_3 to form Na_3TiF_6, followed by the decomposition of $NaBH_4$ due to the presence of the ternary fluoride. Therefore, during heating up to 345 °C, the following reactions can be suggested:

$3NaBH_4 + 2TiF_3 \rightarrow Na_3TiF_6 + TiB + 6H_2$ (+ non-crystalline, B-containing species) (3)

and

$Na_3TiF_6 + NaBH_4 \rightarrow 4NaF + 2H_2$ (+ non-crystalline, Ti- and B-containing species) (4)

At 240 °C and under 140 bar H_2 pressure, no H_2 absorption was observed.

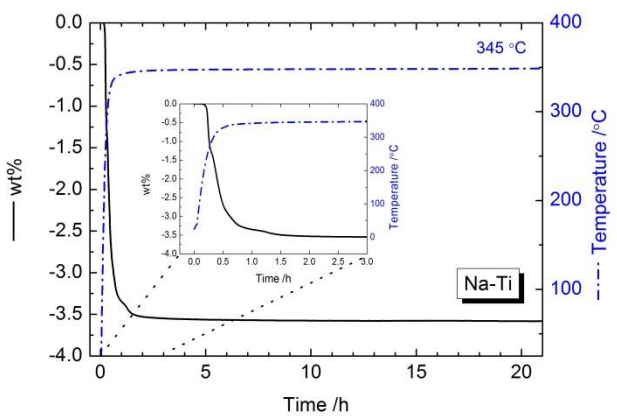

Figure 8: Dehydrogenation profile from RT up to 345 °C of the Na–Ti sample.

In the Na-Mn system (Figure 9), 48 h is not long enough to complete the desorption process at 260 °C. After about 3 h hydrogen release occurs at an almost constant rate. Analogous to the Na–Ti sample (see Eq. 3), this is believed to occur due to the reaction of $NaBH_4$ with MnF_2 to form $NaMnF_3$. Hydrogenation carried out at the same temperature after this

desorption and at 142 bar H_2 reveals a small absorption of 0.25 wt.% H_2 after 48 h. At 360 °C, the Na–Mn system has significantly faster desorption kinetics. 90 % of its total theoretical hydrogen capacity was released in 25 min when the temperature has reached 315 °C. After exposing the dehydrogenated sample to 142 bar of hydrogen at 360 °C, 0.5 wt.% H_2 is absorbed after 48 h. The PXD patterns (not shown here) after dehydrogenation and hydrogenation are identical, suggesting that the limited hydrogen absorption involves only amorphous phases.

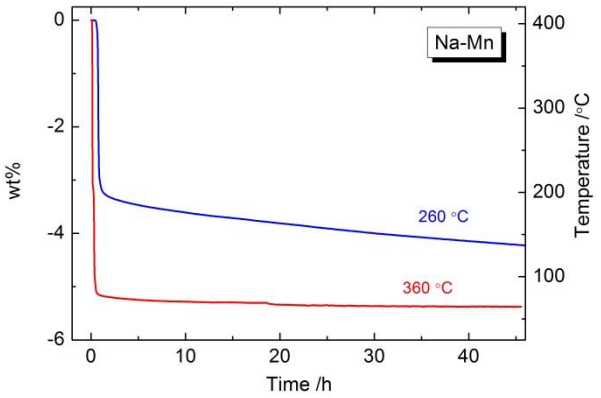

Figure 9: Dehydrogenation profiles acquired from RT up to 260 and 360 °C of the Na–Mn sample.

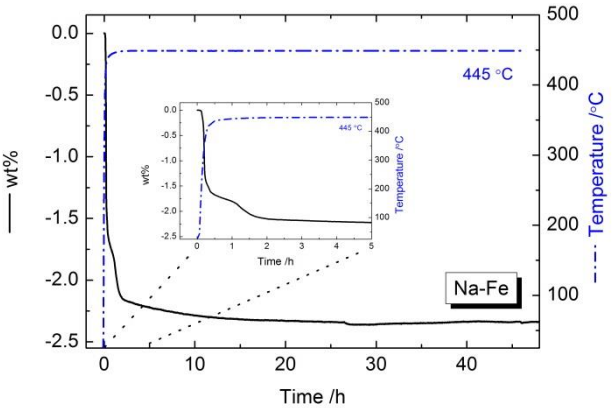

Figure 10: Dehydrogenation profile from RT up to 445 °C of the Na–Fe sample.

For Na-Fe, desorption and absorption measurements were performed at 445 °C (Figure 10). Desorption begins during heating at 180 °C (see inset Figure 10), and thus in very good agreement with the TGA profile. The desorption mechanism involves a 2-step desorption with the second step clearly visible above 380 °C, and thus in good agreement with the TGA data. After 25 h the desorption reaches equilibrium with released 2.6 wt.% H_2 and 85 % being desorbed within 2 h after the beginning of the experiment. Following the desorption the system was exposed to 135 bar of hydrogen at the same temperature. Under these conditions the sample exhibited 1.0 wt.% absorption capacity with very sluggish kinetics.

4 Discussion

The present results show that ball-milling of $NaBH_4$ with TMFs significantly decreases the onset temperature of hydrogen release in comparison to pristine $NaBH_4$. Recently it was suggested that both the cations and anions play a role in the destabilization of the Na–Ti system [51]. After ball-milling the SR-PXD data for the $NaBH_4$-TiF_3 mixture only show crystalline $NaBH_4$ and TiF_3 while with MnF_3 and FeF_3 new phases were observed (Figure 1). The wt.% of FeF_3 was lower than in the starting mixture, and MnF_3 was reduced to MnF_2. This can be related to the relatively high stability of TiF_3 (ΔH_f^0 = -1410 kJ/mol), compared to FeF_3 (ΔH_f^0 = -990.4 kJ/mol) and MnF_3 (ΔH_f^0 = -1071.1 kJ/mol) [54, 55]. Similarly it has been observed that ball-milling results in a reaction between $NaBH_4$ and transition metal chlorides , with lower melting points than the corresponding fluorides [18, 55]. In our Na-Ti sample, a more energetic milling process could possibly change the reaction paths.

The $NaBH_4$:TMF ratio in the starting mixtures was selected to be higher than 3:1, but no formation of mixed-metal borohydrides was observed, as it has been reported for ball-milled alkali metal borohydrides and transition metal chlorides [31, 56]. Instead, during heating, a significant fraction of $NaBH_4$ reacted with the Ti- or Mn-fluoride and formed ternary fluoride compounds. Ball-milling alters the microstructure, and probably this could be the reason of the decreased decomposition temperature of the unreacted $NaBH_4$, compared to the as-received $NaBH_4$. Furthermore, there were no metathesis reactions between cations and anions as suggested by computational DFT screening methods of mixed metal borohydrides [57, 58]. After ball-milling, $NaBF_4$ was found in all samples from the ^{11}B-NMR experiments. The $NaBF_4$:$NaBH_4$ ratios were 1:150, 1:40 and 1:10 for Na-Ti, Na-Mn and Na-Fe, respectively. The amount of $NaBF_4$ formed during ball milling seems to be related to the heat of formation (ΔH_f^0) of each TMF. The lower the ΔH_f^0 value of the TMF the higher the amount of $NaBF_4$ observed in the ^{11}B-NMR spectra of the as-milled samples. Despite minor amounts, one cannot exclude its possible effect on the decomposition pathway or decomposition kinetics of the borohydride. According to the ^{11}B-NMR data, it is an intermediate phase in the decomposition pathway from $NaBH_4$ to NaF and H_2. In addition, $NaBF_4$ seems to contribute to the formation of $NaMnF_3$ for the Na-Mn system (Figure 4). For the as-milled Na–Ti and Na–Fe samples $NaBF_4$ could not be observed by SR-PXD but only by ^{11}B-NMR. For Na-Ti this could be due to the low $NaBF_4$ wt. % and/or the amorphous nature of the phase. Previous investigations on the $NaBH_4$ – TiF_3 system did not report the formation of $NaBF_4$ [51]. Upon heating we also show that the formation of ternary compounds with lower enthalpy of formation/melting points [54, 55] compared to the starting materials significantly affects the temperatures where the main desorption events occur. For Na–Fe, where no intermediate phases are observed, the main fraction of desorbed hydrogen is released approximately 100 °C above the main gas release for the Na–Ti and Na–Mn samples.

Na–Mn shows relatively fast desorption kinetics at both 260 and 360 °C. At 360 °C an almost complete desorption is observed, 80°C below the onset decomposition temperature of the pure borohydride. The reaction kinetics at 260 °C is slower than at 360 °C but still faster than that measured at a higher temperature for Na-Fe. This is likely triggered by the reaction of $NaBH_4$ and MnF_2 to form $NaMnF_3$. At constant temperature the slower desorption probably results from the decomposition

of unreacted $NaBH_4$. Above 400 °C hydrogen release comes from unreacted $NaBH_4$. Finally, at 260 °C the reverse reaction towards $NaBH_4$ does not occur under 142 bar of hydrogen pressure. One can argue that for $NaBH_4$ the relatively high ΔH and ΔS of -108 ± 3 kJ mol^{-1} of H_2 and 133 ± 3 kJ K^{-1} mol^{-1} [59], respectively, require a higher hydrogen pressure to reform the $NaBH_4$ cubic structure. However, we cannot rule out that kinetics barriers may also hinder the hydrogen re-absorption as well.

5 Conclusions

The mechano-chemical reaction between $NaBH_4$ and TMF_3 with TM = Ti, Fe, Mn leads to the formation of composites with a significant reduction of the hydrogen release temperature in comparison to pure $NaBH_4$. In all systems, PXD and ^{11}B-NMR results indicate the formation of $NaBF_4$ which is suggested to play a role in the $NaBH_4$ decomposition. For the Na–Ti sample ^{11}B-NMR revealed the presence of $NaBF_4$ that has not been observed in similar systems before. The ΔH_f^0 value of each TMF is found to be related to the amount of $NaBF_4$ present in the as-milled materials. The formation of the intermediate phases $NaTiF_6$ and $NaMnF_3$ for Na–Ti and Na–Mn, respectively, is found to be beneficial in the decomposition of $NaBH_4$, allowing gas release to begin 210 and 250 °C below the onset decomposition temperature of pure $NaBH_4$. The studied compounds exhibited relatively fast desorption kinetics at 345, 360 and 445 °C for Na–Ti, Na–Mn and Na–Fe, respectively. Furthermore, the last two show slow, limited absorption at the same temperatures. In both samples the absorption does not result in the formation of any crystalline phase. Among the examined TMFs, ball-milling with MnF_3 initiated $NaBH_4$ decomposition at the lowest temperature, whereas TiF_3 displayed the lowest temperature at which the decomposition of $NaBH_4$ was completed. TPD with simultaneous RGA showed that all samples release a minor amount of borane species (B-H) that is in any case two orders of magnitude smaller than the amount of hydrogen. As shown for other systems, TMFs have significant destabilization effect on the $NaBH_4$, and they could play a significant role in the quest of low temperature hydrogen storage systems.

Acknowledgements

Funding from the European Union's Seventh Framework Programme (FP7/2007-2013) for the Fuel Cells and Hydrogen Joint Technology Initiative under the E.U. project SSH2S (grant agreement n. 256653) and the SYNKNØYT program in the Research Council of Norway are acknowledged. The authors thank the project team at the Swiss-Norwegian Beamline at the ESRF, France for their skillful assistance and Ms. Vanessa Lelevrier (Erasmus program, University of Rennes, France) for the ^{11}B-NMR data acquisition.

Notes and references

1. A. Züttel, *Naturwissenschaften*, 2004, **91**, 157-172.
2. L. Schlapbach and A. Züttel, *Nature*, 2001, **414**, 353-358.
3. G. W. Crabtree, M. S. Dresselhaus and M. V. Buchanan, *Phys. Today*, 2004, **57**, 39-44.
4. H. Hagemann and R. Cerny, *Dalton Transactions*, 2010, **39**, 6006-6012.
5. H. W. Li, Y. G. Yan, S. Orimo, A. Züttel and C. M. Jensen, *Energies*, 2011, **4**, 185-214.
6. E. Rönnebro, *Current Opinion in Solid State & Materials Science*, 2011, **15**, 44-51.
7. L. George and S. K. Saxena, *International Journal of Hydrogen Energy*, 2010, **35**, 5454-5470.
8. L. H. Rude, T. K. Nielsen, D. B. Ravnsbæk, U. Bösenberg, M. B. Ley, B. Richter, L. M. Arnbjerg, M. Dornheim, Y. Filinchuk, F. Besenbacher and T. R. Jensen, *Physica Status Solidi a-Applications and Materials Science*, 2011, **208**, 1754-1773.
9. M. D. Riktor, M. H. Sørby, K. Chlopek, M. Fichtner, F. Buchter, A. Züttel and B. C. Hauback, *Journal of Materials Chemistry*, 2007, **17**, 4939-4942.
10. Y. Nakamori, H. W. Li, M. Matsuo, K. Miwa, S. Towata and S. Orimo, *Journal of Physics and Chemistry of Solids*, 2008, **69**, 2292-2296.
11. S. I. Orimo, Y. Nakamori, J. R. Eliseo, A. Züttel and C. M. Jensen, *Chemical Reviews*, 2007, **107**, 4111-4132.
12. T. K. Nielsen, F. Besenbacher and T. R. Jensen, *Nanoscale*, 2011, **3**, 2086-2098.
13. S. Sartori, K. D. Knudsen, Z. Zhao-Karger, E. G. Bardaij, M. Fichtner and B. C. Hauback, *Nanotechnology*, 2009, **20**.
14. H. W. Brinks, A. Fossdal and B. C. Hauback, *Journal of Physical Chemistry C*, 2008, **112**, 5658-5661.
15. M. Corno, E. Pinatel, P. Ugliengo and M. Baricco, *Journal of Alloys and Compounds*, 2011, **509**, S679-S683.
16. J. E. Fonneløp, M. Corno, H. Grove, E. Pinatel, M. H. Sørby, P. Ugliengo, M. Baricco and B. C. Hauback, *Journal of Alloys and Compounds*, 2011, **509**, 10-14.
17. S. Hino, J. E. Fonneløp, M. Corno, O. Zavorotynska, A. Damin, B. Richter, M. Baricco, T. R. Jensen, M. H. Sørby and B. C. Hauback, *Journal of Physical Chemistry C*, 2012, **116**, 12482-12488.
18. I. Llamas-Jansa, N. Aliouane, S. Deledda, J. E. Fonneløp, C. Frommen, T. Humphries, K. Lieutenant, S. Sartori, M. H. Sørby and B. C. Hauback, *Journal of Alloys and Compounds*, 2012, **530**, 186-192.
19. C. Rongeat, I. Lindemann, A. Borgschulte, L. Schultz and O. Gutfleisch, *International Journal of Hydrogen Energy*, 2011, **36**, 247-253.
20. D. B. Ravnsbæk, L. H. Rude and T. R. Jensen, *J. Solid State Chem.*, 2011, **184**, 1858-1866.
21. H. Grove, L. H. Rude, T. R. Jensen, M. Corno, P. Ugliengo, M. Baricco, M. H. Sørby and B. C. Hauback, *Rsc Advances*, 2014, **4**, 4736-4742.
22. L. H. Rude, E. Groppo, L. M. Arnbjerg, D. B. Ravnsbæk, R. A. Malmkjær, Y. Filinchuk, M. Baricco, F. Besenbacher and T. R. Jensen, *Journal of Alloys and Compounds*, 2011, **509**, 8299-8305.
23. L. H. Rude, O. Zavorotynska, L. M. Arnbjerg, D. B. Ravnsbæk, R. A. Malmkjær, H. Grove, B. C. Hauback, M. Baricco, Y. Filinchuk, F. Besenbacher and T. R. Jensen, *International Journal of Hydrogen Energy*, 2011, **36**, 15664-15672.
24. J. E. Olsen, M. H. Sørby and B. C. Hauback, *Journal of Alloys and Compounds*, 2011, **509**, L228-L231.
25. L. H. Rude, U. Filso, V. D'Anna, A. Spyratou, B. Richter, S. Hino, O. Zavorotynska, M. Baricco, M. H. Sørby, B. C. Hauback, H. Hagemann, F. Besenbacher, J. Skibsted and T. R. Jensen, *Physical Chemistry Chemical Physics*, 2013, **15**, 18185-18194.
26. R. H. Heyn, I. Saldan, M. H. Sørby, C. Frommen, B. Arstad, A. M. Bougza, H. Fjellvåg and B. C. Hauback, *Physical Chemistry Chemical Physics*, 2013, **15**, 11226-11230.
27. E. Albanese, G. N. Kalantzopoulos, J. G. Vitillo, E. Pinatel, B. Civalleri, S. Deledda, S. Bordiga, B. C. Hauback and M. Baricco, *Journal of Alloys and Compounds*, 2013, **580**, S282-S286.
28. G. N. Kalantzopoulos, J. G. Vitillo, E. Albanese, E. Pinatel, B. Civalleri, S. Deledda, S. Bordiga, M. Baricco and B. C. Hauback, *Journal of Alloys and Compounds*, 2014.
29. R. Cerny, N. Penin, V. D'Anna, H. Hagemann, E. Durand and J. Ruzicka, *Acta Materialia*, 2011, **59**, 5171-5180.
30. F. Fang, Y. T. Li, Y. Song, J. Zha, B. Zhao and D. L. Sun, *Acta Phys.-Chim. Sin.*, 2011, **27**, 1537-1542.
31. C. Frommen, M. H. Sørby, P. Ravindran, P. Vajeeston, H. Fjellvåg and B. C. Hauback, *Journal of Physical Chemistry C*, 2011, **115**, 23591-23602.

32. M. B. Ley, D. B. Ravnsbæk, Y. Filinchuk, Y. S. Lee, R. Janot, Y. W. Cho, J. Skibsted and T. R. Jensen, *Chem. Mat.*, 2012, **24**, 1654-1663.
33. J. E. Olsen, C. Frommen, M. H. Sørby and B. C. Hauback, *Rsc Advances*, 2013, **3**, 10764-10774.
34. J. E. Olsen, C. Frommen, T. R. Jensen, M. D. Riktor, M. H. Sørby and B. C. Hauback, *Rsc Advances*, 2014, **4**, 1570-1582.
35. I. P. Jain, P. Jain and A. Jain, *Journal of Alloys and Compounds*, 2010, **503**, 303-339.
36. J. Urgnani, F. J. Torres, M. Palumbo and M. Baricco, *International Journal of Hydrogen Energy*, 2008, **33**, 3111-3115.
37. Stasinevich DS and Egorenko GA, *Russian Journal of Inorganic Chemistry*, 1968, **13**, 341.
38. A. R. Yavari, A. LeMoulec, F. R. de Castro, S. Deledda, O. Friedrichs, W. J. Botta, G. Vaughan, T. Klassen, A. Fernandez and Å. Kvick, *Scr. Mater.*, 2005, **52**, 719-724.
39. S. Deledda, A. Borissova, C. Poinsignon, W. J. Botta, M. Dornheim and T. Klassen, *Journal of Alloys and Compounds*, 2005, **404**, 409-412.
40. I. E. Malka, M. Pisarek, T. Czujko and J. Bystrzycki, *International Journal of Hydrogen Energy*, 2011, **36**, 12909-12917.
41. S. A. Jin, J. H. Shim, Y. W. Cho and K. W. Yi, *Journal of Power Sources*, 2007, **172**, 859-862.
42. I. E. Malka, T. Czujko and J. Bystrzycki, *International Journal of Hydrogen Energy*, 2010, **35**, 1706-1712.
43. Z. G. Zhang, H. Wang and M. Zhu, *International Journal of Hydrogen Energy*, 2011, **36**, 8203-8208.
44. S. Srinivasan, D. Escobar, Y. Goswami and E. Stefanakos, *International Journal of Hydrogen Energy*, 2008, **33**, 2268-2272.
45. T. D. Humphries, G. N. Kalantzopoulos, I. Llamas-Jansa, J. E. Olsen and B. C. Hauback, *The Journal of Physical Chemistry C*, 2013, **117**, 6060-6065.
46. J. F. Mao, X. B. Yu, Z. P. Guo, H. K. Liu, Z. Wu and J. Ni, *Journal of Alloys and Compounds*, 2009, **479**, 619-623.
47. C. M. Araújo, R. Ahuja, A. V. Talyzin and B. Sundqvist, *Physical Review B*, 2005, **72**, 054125.
48. J. Huot, D. B. Ravnsbæk, J. Zhang, F. Cuevas, M. Latroche and T. R. Jensen, *Progress in Materials Science*, 2013, **58**, 30-75.
49. A. P. Hammersley, ``*FIT2D: An Introduction and Overview*'', *ESRF97HA02T*, 1997.
50. J. Rodriguez-Carvajal, *Physica B*, 1993, **192**, 55-69.
51. J. F. Mao, Z. P. Guo, I. P. Nevirkovets, H. K. Liu and S. X. Dou, *Journal of Physical Chemistry C*, 2012, **116**, 1596-1604.
52. M. D. Riktor, Y. Filinchuk, P. Vajeeston, E. G. Bardaji, M. Fichtner, H. Fjellvåg, M. H. Sørby and B. C. Hauback, *Journal of Materials Chemistry*, 2011, **21**, 7188-7193.
53. V. Amirthalingam, M. D. Karkhanavala and U. R. K. Rao, *Z. Kristall.*, 1980, **152**, 57-61.
54. http://webbook.nist.gov.
55. R. H. Perry and D. W. Green, *Perry's Chemical Engineers' Handbook (7th Edition)*, McGraw-Hill1997.
56. R. Cerny, G. Severa, D. B. Ravnsbaek, Y. Filinchuk, V. D'Anna, H. Hagemann, D. Haase, C. M. Jensen and T. R. Jensen, *Journal of Physical Chemistry C*, 2010, **114**, 1357-1364.
57. D. S. Aidhy and C. Wolverton, *Physical Review B*, 2011, **83**.
58. J. S. Hummelshøj, D. D. Landis, J. Voss, T. Jiang, A. Tekin, N. Bork, M. Dulak, J. J. Mortensen, L. Adamska, J. Andersin, J. D. Baran, G. D. Barmparis, F. Bell, A. L. Bezanilla, J. Bjork, M. E. Bjorketun, F. Bleken, F. Buchter, M. Burkle, P. D. Burton, B. B. Buus, A. Calborean, F. Calle-Vallejo, S. Casolo, B. D. Chandler, D. H. Chi, I. Czekaj, S. Datta, A. Datye, A. DeLaRiva, V. Despoja, S. Dobrin, M. Engelund, L. Ferrighi, P. Frondelius, Q. Fu, A. Fuentes, J. Furst, A. Garcia-Fuente, J. Gavnholt, R. Goeke, S. Gudmundsdottir, K. D. Hammond, H. A. Hansen, D. Hibbitts, E. Hobi, J. G. Howalt, S. L. Hruby, A. Huth, L. Isaeva, J. Jelic, I. J. T. Jensen, K. A. Kacprzak, A. Kelkkanen, D. Kelsey, D. S. Kesanakurthi, J. Kleis, P. J. Klupfel, I. Konstantinov, R. Korytar, P. Koskinen, C. Krishna, E. Kunkes, A. H. Larsen, J. M. G. Lastra, H. Lin, O. Lopez-Acevedo, M. Mantega, J. I. Martinez, I. N. Mesa, D. J. Mowbray, J. S. G. Myrdal, Y. Natanzon, A. Nistor, T. Olsen, H. Park, L. S. Pedroza, V. Petzold, C. Plaisance, J. A. Rasmussen, H. Ren, M. Rizzi, A. S. Ronco, C. Rostgaard, S. Saadi, L. A. Salguero, E. J. G. Santos, A. L. Schoenhalz, J. Shen, M. Smedemand, O. J. Stausholm-Moller, M. Stibius, M. Strange, H. B. Su, B. Temel, A. Toftelund, V. Tripkovic, M. Vanin, V. Viswanathan, A. Vojvodic, S. Wang, J. Wellendorff, K. S. Thygesen, J. Rossmeisl, T. Bligaard, K. W. Jacobsen, J. K. Norskov and T. Vegge, *Journal of Chemical Physics*, 2009, **131**.
59. P. Martelli, R. Caputo, A. Remhof, P. Mauron, A. Borgschulte and A. Züttel, *Journal of Physical Chemistry C*, 2010, **114**, 7173-7177.